Inclined wall friction test 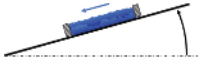	Scale invariant.	Direct measurement of the static friction angle; Measure the sliding or rolling speed to estimate the coefficient of dynamic friction and rolling friction, respectively.	The test setup is more complex to manufacture, if a manual process is not to be followed. The angle of the wall needs to be adjusted using a very slow and smooth action. For this purpose a dedicated motor- or mechanical drive is needed. The tests are simple and quick to execute. Suitable for all particle sizes. Rolling friction can only be estimated for (close to) spherical particle shapes.	Direct measurement of parameter values; hence, no need to replicate the test in a DEM simulation (DMA). For further information see: Barrios et al. [51], Wang et al. [39], Hlosta et al. [47], Agarwal et al. [52].
Direct shear tests 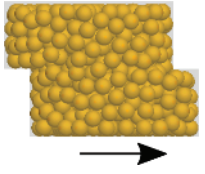	Scale variant.	Angle of internal friction; cohesion (apparent cohesion for non-cohesive materials); dilatant behaviour; material-wall friction angle.	The test apparatus is complex and should be carefully manufactured or, preferably, a commercial unit should be used. Tests are cumbersome to execute and require multiple steps (simulations and experimentally). Limited maximum particle size dependent on the available test cells (experiment). For a given maximum particle size, all PSDs can be accommodated.	To obtain a full yield locus, a series of tests are required which can take long to complete (simulations and experimentally). For detailed procedures, refer to the various standards, such as ASTM D3080/D3080M [53] and ISO 17892-10:2018 [54] for the translational Jenike shear tester, and ASTM D6773-16 [55] for the Schulze ring shear tester (rotational). These standard test procedures require several steps such as pre-shear and shear, especially for cohesive materials. For further information see: Coetzee [11, 18], Mohajeri et al. [25, 57], Simons et al. [56], Bian et al. [58] and Falke et al. [59], Grima and Wypych [60].

(Continued)

Table 1.2 (Continued)

Calibration test	Test properties: Scale effects	Test properties: Bulk measures for calibration	Test effort, applicability	Comments and further references
Confined uniaxial compression test 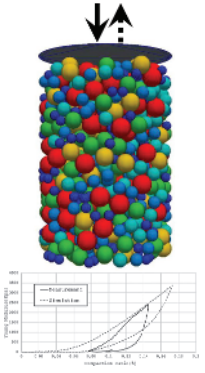	Scale invariant if the container is sufficiently large to accommodate enough particles per cross section.	Bulk stiffness.	Although the cylindrical container is simple and easy to manufacture, the test requires a universal tensile/compression or similar test machine. The simulation is easy to set up. The tests are simple and quick to execute. Suitable for all sample and PSD sizes, by selecting an appropriate container size.	Note that this test should not be confused with the uniaxial compression test [UCT] often used to measure the flow function (unconfined compression strength) of cohesive materials (mainly powders). In the UCT, the sample is first compressed (consolidated) under confined conditions, after which the same sample is compressed under unconfined conditions. If a tensile/compression machine is not available, dead loads can be used to apply the normal load incrementally. This is not ideal, but can provide enough information to estimate bulk stiffness. For further information see: Coetzee [11, 18], Lommen et al. [27], Thakur et al. [61], Donohue et al. [62].
Drop and pendulum tests 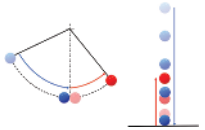	Scale invariant.	Particle–particle coefficient of restitution; particle–wall coefficient of restitution.	The tests are relatively easy and simple to execute, but a means to optically measure the particle motion is needed. Suitable for all particle sizes. Drop tests are not suitable for non-spherical particles, unless very sophisticated equipment and techniques are available to measure the 3D particle trajectory and spin.	Direct measurement of parameter values; hence, no need to replicate the test in a DEM simulation (DMA) For further information see: Barrios et al. [51], Yurata et al. [63], Hastie [64], Hlosta et al. [65], Elskamp et al. [37].

Penetration test 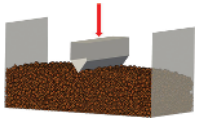	Scale variant due to the ratio of the tip to particle size.	Penetration resistance (resistance of the tip and shaft can be measured independently). If a transparent container is used, and the particles are coloured by layer, the flow field can be observed and measured.	The test apparatus is complex and requires an actuator to push the penetrometer into the material bed at a constant speed. The simulation is easier to set up. The tests are simple and quick to execute. Requires a large sample to cover the container. Suitable for all PSDs.	The container should be large enough to eliminate any wall boundary effects. For further information see: Mohajeri et al. [66, 67], Lommen et al. [42], Coetzee and Els [10].

1.7 Recommended Calibration Procedure for Non-cohesive and Slightly Cohesive Materials

As described earlier, the contact model parameters need to be determined by running a series of DEM simulations with varying parameters. The parameters can be varied systematically or through an optimisation algorithm. Ideally, in both approaches, an automated post-processing of the model results is required since a manual process would not be feasible for a large number of simulations.

The systematic variation of the parameter values over a whole range is time-consuming due to the high number of independent simulations required. However, this approach provides a deep understanding of the general relation between the simulated macroscopic (bulk) behaviour and the (individual) input parameters. Hence, this section focuses on the systematic approach, while Section 1.8 provides an overview of optimisation algorithms.

1.7.1 Ambiguous Parameter Combinations

The ideal situation would be to have an experiment of which the result is dependent on only a single parameter. If such an experiment is available for each of the unknown parameter values, calibration would be straightforward. Unfortunately, most numerical experiments are, however, sensitive to more than one parameter. As an example, take the very common AoR lifting cylinder test. Wensrich and Katterfeld [17] showed that (for non-cohesive materials) the AoR is dependent on both the particle–particle coefficient of sliding friction μ_{P} and the coefficient of rolling friction μ_{r}. When such results are plotted, a contour diagram results, which typically looks like the graph presented in Figure 1.3.

Figure 1.3 clearly demonstrates that there are an infinite number of parameter (μ_{P} and μ_{r}) combinations which result in the same value of the macroscopic AoR. This example highlights the problem of ambiguous parameter combinations. One calibration test result cannot provide a unique set of two (or more) contact model parameters. Hence, several test results are necessary to find a unique parameter set. The following section describes a procedure which solves the problem of ambiguous parameter combinations for non-cohesive materials.

This approach can also work for ‘slightly’ cohesive materials. However, with increasing bulk cohesive behaviour, the material flow increases in complexity and the test results are usually less consistent. Therefore, a larger number of tests are required to decrease the parameter range. To illustrate this point, a comparison of the AoR test with and without cohesion is shown in Figure 1.4. The calibration of cohesive materials is described in more detail in Section 1.7.

1.7.2 Solving for an Unambiguous Parameter Combination

The problem of ambiguous parameter combinations is equivalent to simultaneously solving a set of mathematical equations with a number of unknown variables or (calibration) parameters. A unique solution can only be obtained if the number of

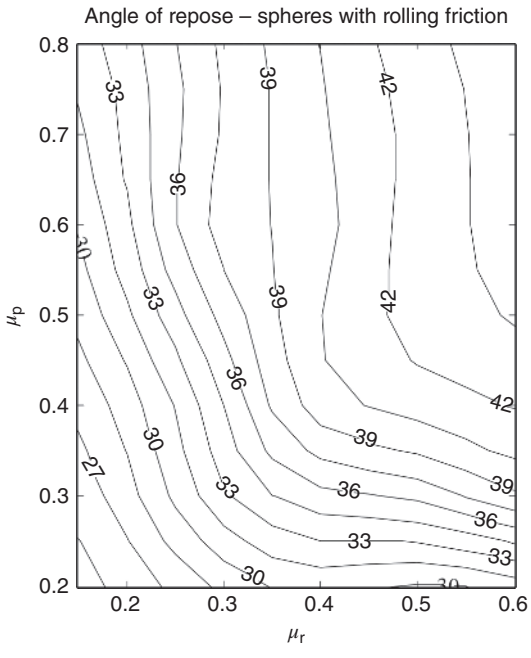

Figure 1.3 AoR simulation results according to Wensrich and Katterfeld et al. [17] using a lifting cylinder test for a systematic variation of particle–particle sliding friction μ_P and rolling friction μ_r. A constant macroscopic AoR is represented by an isoline. No cohesion was considered.

independent equations is equal to the number of variables. Using this analogy, the calibration test(s) should produce the same number (or more) of 'independent' test results as the number of DEM parameters to which the model is sensitive. The explanation in Section 1.4 and the summary in Table 1.1 help to identify the most influential parameter(s) for a given bulk property.

This analogy clearly explains why calibration tests which produce more than one test result (or bulk measure) are preferred. For example, the draw down test and the direct shear test produce four results each. However, not all of the test results can be called independent. For instance, the two AoR results and the remaining mass in the upper or lower chamber of the draw down test are dependent on each other. The higher the AoR in the upper chamber, the higher is the remaining mass in that chamber, and vice versa. In the direct shear test, the shear response at different normal stresses can be used as well as the internal friction angle and the time to reach failure.

For each bulk measure (either from a single test or multiple tests), a diagram such as the one presented in Figure 1.3 can be produced. The diagrams can then be superimposed to obtain a unique or unambiguous set of parameter values, i.e. a single set of parameter values which satisfies all test results. However, there is no guarantee that, in all cases, the isolines (one for each bulk measure) will intersect at a single point as described in Derakhshani et al. [36]. Often the measurement error needs to be considered to ensure a significant overlap of the test results as shown in detail by Roessler et al. [14].

Figure 1.5 shows how the different draw down test results (shear angle in the upper chamber, AoR in the lower chamber, mass in the lower chamber, and mass

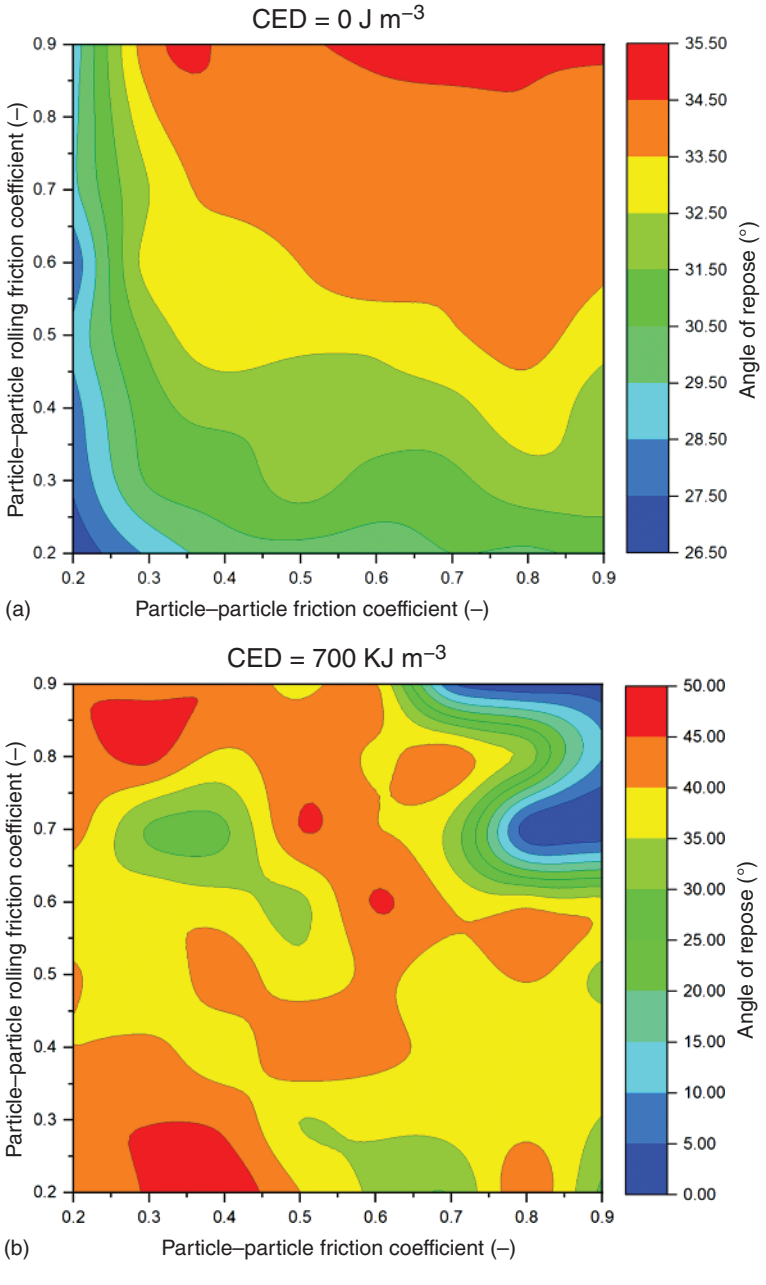

Figure 1.4 Comparison of AoR simulation results with varying particle–particle (sliding) friction and rolling friction coefficient for non-cohesive (a) and cohesive materials (b). Similar to Pachon-Morales et al. [43] for non-cohesive and slightly cohesive materials, a direct relation between the frictional values and the AoR can be shown. This is not the case for the cohesive material where a more irregular and complex behaviour can be seen.

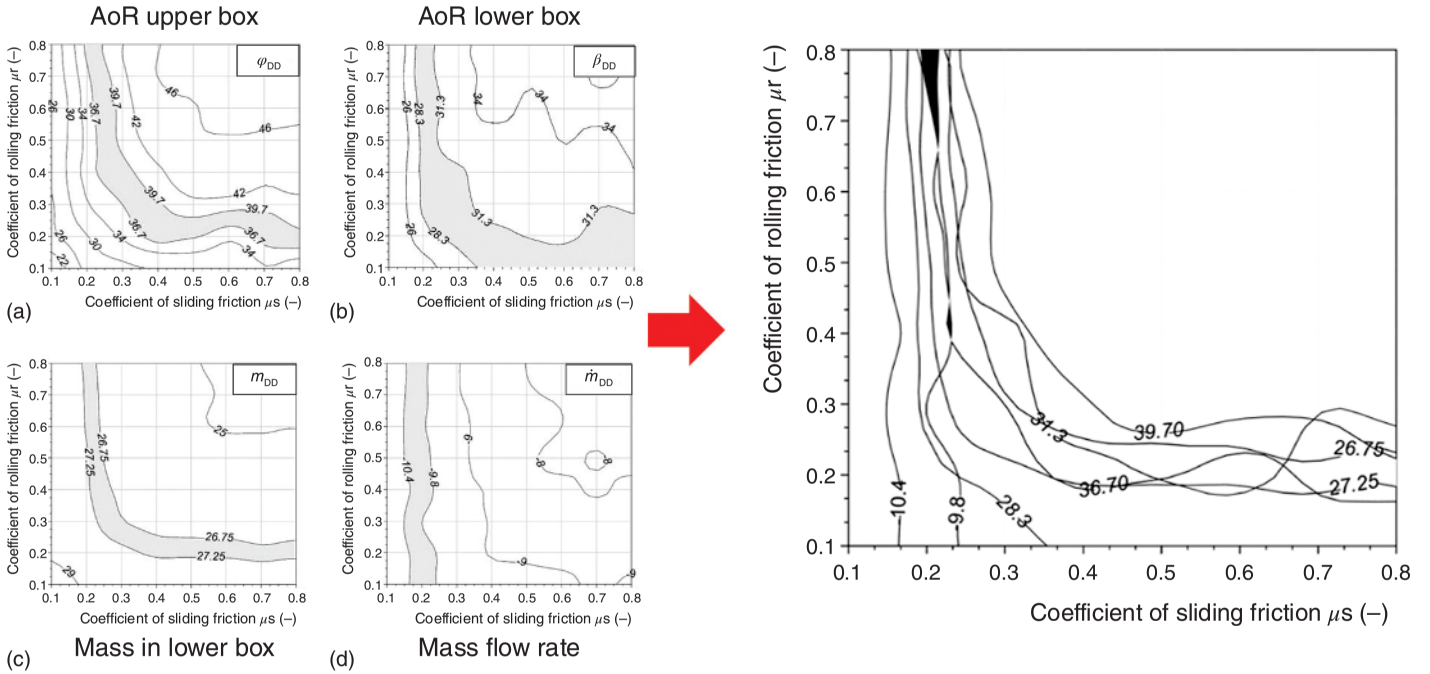

Figure 1.5 Combination of draw down test results for gravel with consideration of the measurement error for the identification of a unique parameter set. Source: Adapted from Roessler et al. [14].

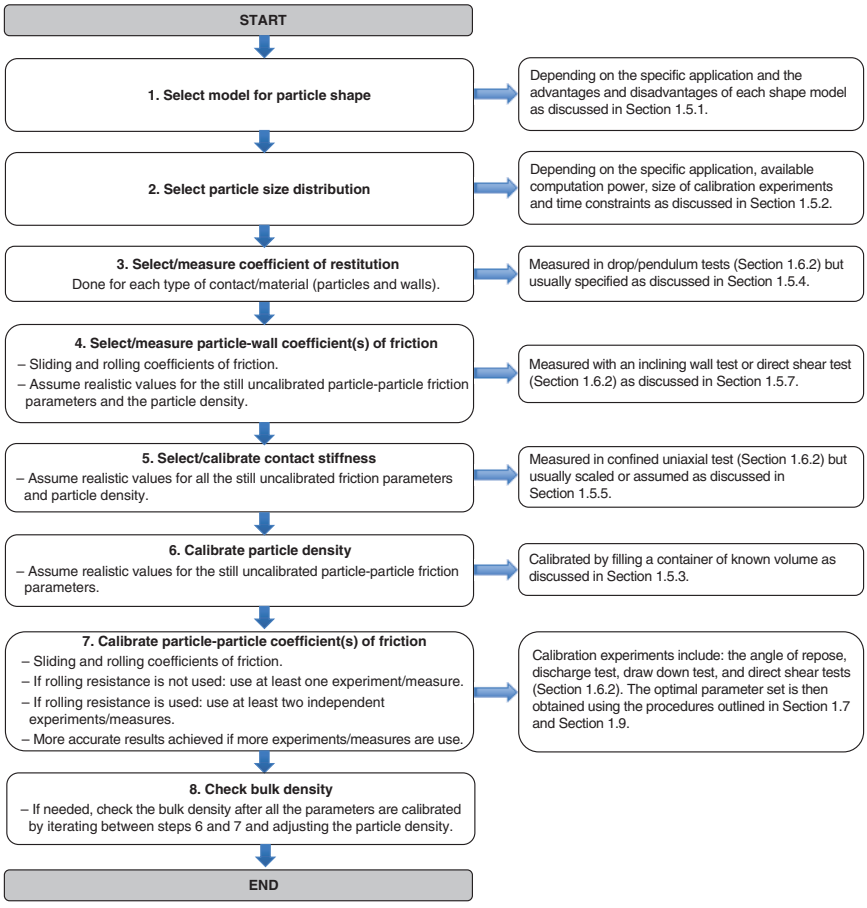

Figure 1.6 Calibration procedure for non-cohesive materials. Source: Adapted from Katterfeld et al. [28].

flow rate) can be plotted by taking the measurement error (grey marked areas in the diagrams on the left) into account. This significantly decreases the number of possible parameter combinations (sliding and rolling friction in this case) if the isolines of the contour plots are then overlaid as shown in the diagram on the right-hand side. The small black area in the right-hand side diagram shows the possible combination of the sliding and rolling friction which results in the same realistic shear angle, AoR, mass in the lower chamber, and the mass flow rate as measured in the experiment. Within the black area, the calculated cumulated error between simulated and measured test result allows the identification of a single parameter set.

The steps required to identify a unique set of DEM parameters can be summarised as follows:

1. Make use of a single calibration test with several independent bulk measures or a number of calibration tests, each with a single result or bulk measure. The latter case requires more effort in terms of experiments and simulations.

2. Determine the measurement errors for each test result (bulk measure) and consider them in the analysis of the DEM results.
3. Identify the parameter ranges which provide realistic simulation results for each test.
4. Calculate the cumulative error between simulation results and experimental measurements and identify the parameter set with a minimum error.

In the given examples of the lifting cylinder test (Figure 1.3) and the draw down test (Figure 1.5), only the influence of the particle–particle coefficients of sliding and rolling friction was shown. Although these two parameters are the ones which have the most significant influence on the modelled bulk behaviour of non-cohesive materials, the other parameters should also be carefully considered. This leads to the obvious question: is it necessary to vary all these parameter values systematically? This would require a tremendous number of independent simulation runs, which is not feasible. However, it has been shown that if the calibration procedure of individual parameters is executed in a specific sequence, the need for iterations and finding the unique (optimal) set of parameters can be minimised.

Based on the experience of a large number of academic and industrial experts, the calibration procedure as shown in the flowchart in Figure 1.6 was developed for non-cohesive materials, as presented in Katterfeld et al. [28]. The flowchart includes references to the sections where the influence of the specific parameter on the bulk behaviour is explained as well as the proposed experiment(s) to calibrate each parameter.

1.8 Outlook on the Calibration of Cohesive Materials

Cohesion, usually through the effects of moisture, can significantly alter the bulk behaviour of granular materials. However, the DEM research and modelling community do not yet have the same level of confidence in any DEM model to accurately predict the bulk behaviour of cohesive materials compared to that of non-cohesive materials. The exact reason for this is not known, and it might be that we are not yet able to successfully calibrate the cohesive parameters, and/or the cohesive contact models that are currently available do not capture the real physics accurately enough. For completeness, a short summary of the published attempts made to calibrate cohesive materials is presented here.

Grima [68] and Grima and Wypych [49] developed and validated a strategy for calibrating the parameters of dry and wet black coal and bauxite. First, the material was calibrated in a dry non-cohesive state based on flow property measurements and bench scale tests and using the Hertz–Mindlin (no slip) contact model. Thereafter, the material was tested in a moist cohesive state and the appropriate cohesive parameters introduced to the DEM contact model. The cohesive parameters were calibrated, while the non-cohesive parameter values remained unchanged. Two experimental tests were used to calibrate the parameters. First, a swing-arm slump test with a split cylinder was developed to measure the AoR. The second test was

based on a cylindrical draw down test, where the shear angle (upper box), poured AoR (lower box), and the mass flow rate (estimated from high-speed photography) were measured. In addition, the impact force of the material onto the bottom plate was measured.

Due to the cohesive effects, the shape of the formed piles was irregular, which made it difficult to define the AoR in the slump test. A quantitative approach was then followed, and the general shape of the heap used for comparison. In the draw down test, the cohesive material slumped down onto the lower plate, and the cohesive parameter (the cohesive energy density) had no significant effect on the poured AoR. However, it had a significant effect on the shear angle, and in the end, this was the only measured parameter from the draw down test that could be used for calibration purposes. However, a single value of the cohesion energy density, which accurately predicted the slump test AoR and the draw down shear angle, could not be found. In the end, the study concluded that a calibrated cohesion parameter for one system might not be suitable for another system.

Katterfeld et al. [69] used two different cohesive contact models and the draw down test to calibrate the parameters for wet gypsum. Both models under-predicted the shear angle in the upper box of the draw down test and over-predicted the poured AoR in the lower box.

Roessler and Katterfeld [29] made use of the lifting cylinder test to calibrate the cohesive parameter for wet sand. The AoR showed a very high level of variability, ranging from 40.4° to 84.3° for the same material in repeated tests. Hence, the macroscopic flow behaviour was rather analysed where three distinct and reproducible phases could be identified during the upward motion of the cylinder and used as calibration criteria. This study, however, made use of a single moisture content, and this approach still needs to be verified for different moisture contents and different bulk materials.

Ajmal et al. [70], on the other hand, showed that the draw down test could be used to successfully calibrate sliding friction, rolling friction, and cohesion parameter for wet sand (10% moisture content). It was shown that the blockage or arching of material at the opening was independent of sliding and rolling friction and depended only on the cohesion parameter. Comparing these results to experimental observations for various opening sizes, a narrow band of values for the cohesion parameter could be established. A unique set of parameter values could then be obtained by comparing the AoR, formed in the lower box, and the total mass that flowed to the bottom box, to experimental measurement. It was noted that the shear angle, formed in the upper box, could not be used since it was not reproducible.

Mohajeri et al. [57] used the ring shear test to calibrate the parameters of cohesive (moist) coal by using an elasto-plastic cohesion contact model. This work was further extended [71] in a study where a combination of calibration experiments was used to calibrate the parameters of cohesive iron ore. The tests included a ring shear test, a shear box (ledge AoR), and a penetration test.

Carr et al. [72] investigated the use of two contact models to simulate the behaviour of cohesive iron ore with varying moisture content. The material was allowed to flow from a feeding conveyor onto an impact plate, where the build-up of material was observed. It was concluded that only the liquid-bridge model was capable of

simulating the clumping effect of the material which was observed during the experiments. In a further study [73], a combination of the shear box (ledge test), draw down, and a conveyor impact plate test was used. By varying the cohesive parameter, the draw down test was used to investigate flowing and arching cases. The irregular slopes that formed made it difficult to measure the angles, and it was concluded that in the shear box and the draw down test, the residual mass was a more definite and reproducible calibration measure.

1.9 Optimisation Approaches Applied to the Calibration Process

An increasing number of calibration parameters increases the problem of ambiguous parameter sets and brings classical visualisation techniques such as the contour plots, shown in Section 1.6, to their limits. Hence, if more than two parameters should be calibrated, for example, if one would include cohesion or particle upscaling, the use of optimisation algorithms might be mandatory. Also, an increasing number of calibration test results such as an AoR, shear angle, and mass flow rate from a draw down test or different yield loci from a direct shear test lead to complex analyses with a lot of processing steps. The aim of the calibration process is to find a set of DEM parameter values in such a way that the simulation results of the physical calibration experiments are the most accurate (optimal) as compared to the experimental results. Hence, the task of the optimisation process is to minimise the difference between the experimental and simulation results.

It was already discussed that multiple calibration test results are necessary for finding an unambiguous parameter set. The calibration test results are the so-called objective function values or target values for the optimisation algorithm. Hence, only such algorithms can be used which can handle multiple target values. However, besides the problem of handling multiple parameters and multiple target criteria, the biggest advantage of optimisation algorithms is the reduced number of calibration simulations. This addresses one of the largest bottlenecks in the whole calibration process, namely the time required to run a whole series of calibration simulations.

Different optimisation schemes are available, and Richter et al. [74] identified the following characteristics of typical DEM results as significant to consider in the selection process:

- nonlinear objective function topology,
- expensive computation,
- gradients cannot be obtained directly,
- limitations of the search space in the form of parameter boundaries (restricted optimization problem),
- there can be more than one optimum or many local optima,
- rough objective function surface due to stochastic effects and numerical noise,
- more than one objective function value is necessary for calibration,
- discontinuities can occur (e.g. bridging in funnel flow experiments due to high friction values).

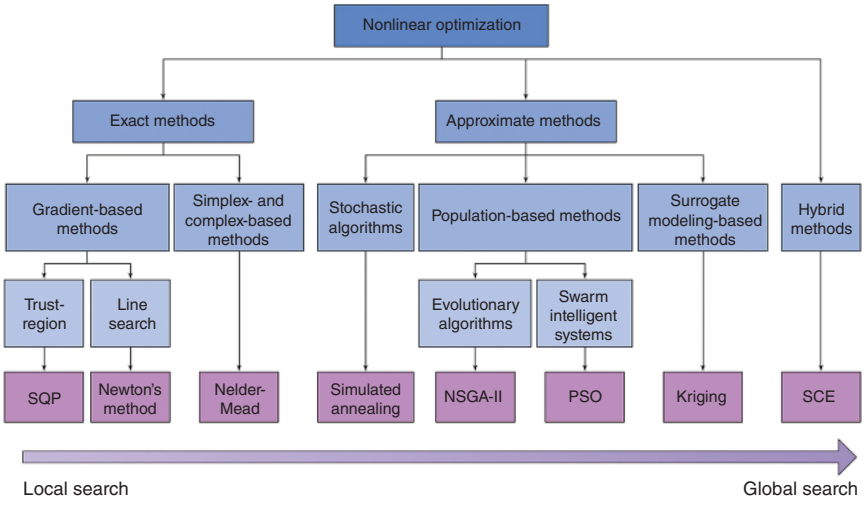

Figure 1.7 Overview of optimisation algorithm. SQP = sequential quadratic programming, NSGA = non-dominated sorting genetic algorithm, PSO = particle swarm optimization, SCE = shuffled complex evolution. Source: Richter et al. [74]/with permission of Elsevier.

Richter et al. [74] also provides a comprehensive overview of the different optimisation approaches which are generally known (Figure 1.7). A systematic review of these approaches is essential since different terms are used in literature for the same optimisation approach. For example, Hess et al. [75] used the term particle swarm optimisation whereas Do et al. [35] used the term genetic algorithms.

An increasing number of publications explain the use of 'Artificial Intelligence' or 'Machine Learning' to optimise the calibration process. However, often the actual algorithm used is similar to those from publications which make use of different terms.

For the DEM application, the use of surrogate models can be identified as one of the best optimisation approaches. Many DEM publications focus on this approach. Most surrogate models are capable of identifying a global optimum on a rough objective function surface with many local optima within a few iterations. Further, they can consider parameter limitations and multi-objective problems and discontinuities.

The surrogate model approach generates, in the first step, a virtual approximation of the objective functions. Only a few calibration simulations are necessary for this. The sampling method for selecting the initial parameters is an important step. Based on the generated surrogate model, a set of optimised parameters is predicted and evaluated by the so-called acquisition function. Then, an additional calibration simulation is undertaken, and the difference to the target values is calculated. If the difference is larger than stopping criteria, the surrogate model is refined by the new simulation results and the whole process is repeated. Richter et al. [74] have suggested a general description of the necessary steps to use the surrogate model approach. The flow diagram in Figure 1.8 summarises the flow of the so-called Generalised Surrogate Modelling-based Calibration (GSMC).

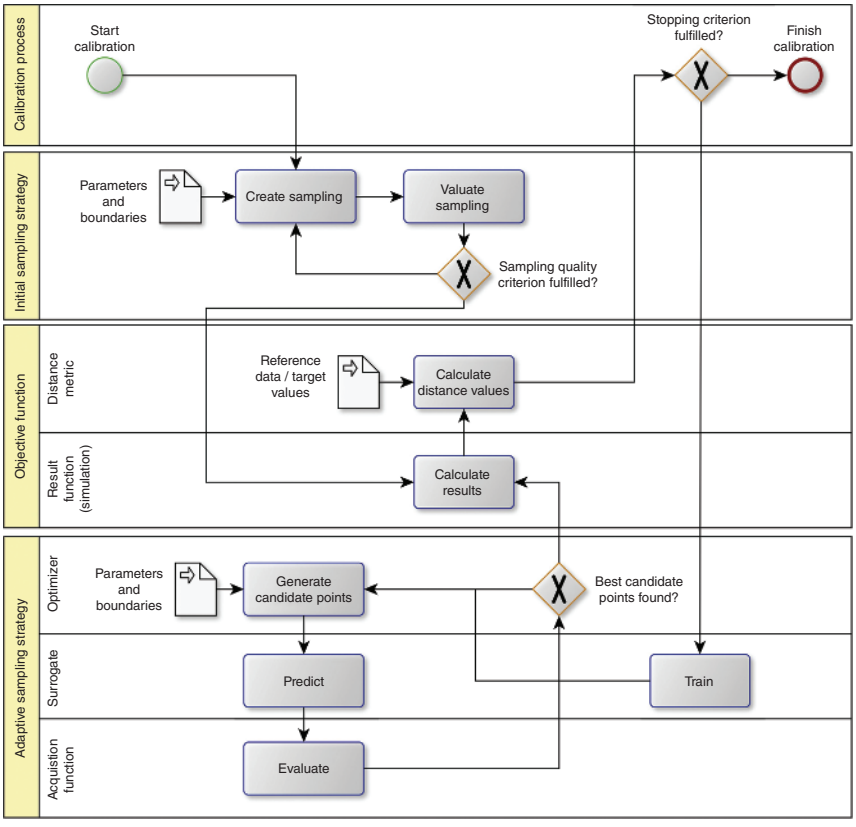

Figure 1.8 Component structure and process of generalised surrogate modelling-based calibration (GSMC). Source: Richter et al. [74]/with permission of Elsevier.

To calculate and predict the surrogate model, several approaches are known. They can be separated in probabilistic and non-probabilistic approaches. Probabilistic surrogate models include the calculation of the probability for the prediction of the estimated value, which provides advantages in the evaluation process. Richter et al. [74] have analysed a number of different surrogate algorithms, which include Gaussian process regression (GPR), artificial neural networks, multi-adaptive regression splines, and universal Kriging. Rackl and Hanley [76] and Kriging and Benvenuti et al. [77] used artificial neural networks. Richter et al. [74] could achieve the best results with the GPR which belongs to the probabilistic approaches. Due to the probabilistic surrogate model and the probabilistic acquisition function, the approach can be classified as a Bayesian optimisation approach. This approach and the Gaussian model were also used by Hartmann et al. [78].

Since Richter et al. [74] and Roessler et al. [14] used the same calibration tests and data, it could be shown that the use of the optimisation algorithm resulted in the same final DEM parameter set as the systematic parameter selection process where a full factorial design was used. While the systematic selection process required at least 64 simulation runs, the GSMC with GPR needed less than 23 simulation runs.

1.10 Conclusion

This chapter discusses one of the most important requirements for the successful application of the DEM: an understanding of how the DEM parameters influence the bulk behaviour of granular materials, and why a calibration of these parameters is absolutely necessary if accurate simulation results are to be achieved. The most important parameters used in almost all DEM models were presented, and their general influence on simulated results was discussed.

The most commonly used calibration tests were described as well as the problem of ambiguous parameter sets, which require calibration tests with several measurable outcomes (bulk measures). A standard process for the calibration of non- and slightly cohesive materials was presented, and it was discussed why the calibration of cohesive materials is much more problematic and still a matter of research.

Finally, the use of optimisation algorithms for an efficient calibration process was described. Such algorithms might be an essential prerequisite for the complex task of calibrating cohesive materials.

Although the calibration process is essential for the successful application of DEM, no available DEM software addresses this issue with a predefined workflow, including both pre- and postprocessing. Most DEM software have a batch feature to run a series of simulations with automated parameter variation. For the automated calibration using optimisation algorithms, open source software packages such as Decalioc or GrainLearning exist, but they demand a deep understanding of the whole procedure and require programming skills.

This is one reason why the calibration of DEM parameters – although very necessary and important – is often performed by experts in the field as a consulting service. Such services must include suitable experimental tests and the run and analysis of a series of calibration simulations. Experience proves that, with the current state of the art in DEM calibration, knowledge of the physical behaviour of bulk materials in close combination with simulation know-how is required to obtain accurate calibration results. However, metamodel-based approaches like those described by Richter and Will [79] might lead to an improved understanding of the DEM parameters and their influence on the macroscopic behaviour of bulk materials and, in the future, significantly reduce the complexity of the calibration process.

Glossary

Angle of repose
Bulk calibration approach
Bulk cohesion
Bulk density
Bulk friction
Bulk stiffness
Calibration philosophies
Calibration process
Calibration test

Coarse graining
Coefficient of restitution
Cohesive material
Combined scaling
Contact damping
Contact model
Contact properties
Contact stiffness
DEM parameters
Direct measurement approach
Dissipation of energy
Draw down test
Exact scaling
Hybrid scaling
Lifting cylinder
Multi-sphere particle
Non-cohesive material
Optimisation
Parameter combination
Parameter set
Particle density
Particle shape
Particle size distribution
Physical bulk properties
Porosity
Rolling friction
Scalping
Sliding friction

References

1 Coetzee, C.J., Basson, A.H., and Vermeer, P.A. (2007). Discrete and continuum modelling of excavator bucket filling. *Journal of Terramechanics* 44: 177–186.
2 Cundall, P.A. and Strack, O.D. (1979). Discrete numerical model for granular assemblies. *Géotechnique* 29 (1): 47–65.
3 O'Sullivan, C. (2011). *Particulate discrete element modelling, a geomechanics perspective, Applied Geotechnics*, vol. 4. London and New York: Spon Press ISBN13: 978-0-203-88098-2.
4 Thornton, C. (2015). *Granular dynamics, contact mechanics and particle system simulation, A DEM study*. Cham: Springer ISBN 978-3-319-18710-5.
5 Hazzar, L., Nuth, M., and Chekired, M. (2020). DEM simulation of drained triaxial tests for glass-beads. *Powder Technology* 364: 123–134.
6 Mesnier, A., Peczalski, R., Mollon, G., and Vessot-Crastes, S. (2020). Mixing of bi-dispersed milli-beads in a rotary drum: mechanical segregation analyzed by lab-scale experiments and DEM simulation. *Processes* 8 (9): 1166.

7 Coetzee, C.J. (2017). Review: calibration of the discrete element method. *Powder Technology* 310: 104–142.

8 Mitarai, N. and Nori, F. (2006). Wet granular materials. *Advances in Physics* 55 (1, 2): 1–45.

9 Seville, J.P.K., Willet, C.D., and Knight, P.C. (2000). Interparticle forces in fluidisation: a review. *Powder Technology* 113: 261–268.

10 Coetzee, C.J. and Els, D.N.J. (2009). Calibration of discrete element parameters and the modelling of silo discharge and bucket filling. *Computers and Electronics in Agriculture* 65: 198–212.

11 Coetzee, C.J. (2020). Calibration of the discrete element method: strategies for spherical and non-spherical particles. *Powder Technology* 364: 851–878.

12 Guo, Y., Zhao, C., Markine, V. et al. (2020). Discrete element modelling of railway ballast performance considering particle shape and rolling resistance. *Railway Engineering Science* 28: 382–407.

13 Markauskas, D., Ramírez-Gómez, A., Kacianauskas, R., and Zdancevicius, E. (2015). Maize grain shape approaches for DEM modelling. *Computers and Electronics in Agriculture* 118: 247–258.

14 Roessler, T., Richter, C., and Katterfeld, A. (2019b). Development of a standard calibration procedure for the DEM parameters of cohesionless bulk materials. Part I - solving the problem of ambiguous parameter combinations. *Powder Technology* 343: 803–812.

15 Wensrich, C.M., Katterfeld, A., and Sugo, D. (2014). Characterisation of the effects of particle shape using a normalised contact eccentricity. *Granular Matter* 16 (3): 327–337.

16 Ai, J., Chen, J.F., Rotter, J.M., and Ooi, J.Y. (2011). Assessment of rolling resistance models in discrete element simulations. *Powder Technology* 206: 269–282.

17 Wensrich, C. and Katterfeld, A. (2012). Rolling friction as a technique for modelling particle shape in DEM. *Powder Technology* 217: 409–417.

18 Coetzee, C.J. (2016). Calibration of the discrete element method and the effect of particle shape. *Powder Technology* 297: 50–70.

19 Stahl, M. and Konietzky, H. (2011). Discrete element simulation of ballast and gravel under special consideration of grain-shape, grain-size and relative density. *Granular Matter* 13: 417–428.

20 Chen, W., Donohue, T., Katterfeld, A., and Williams, K. (2017). Comparative discrete element modelling of a vibratory sieving process with spherical and rounded polyhedron particles. *Granular Matter* 19 (81) 1–12.

21 Alonso-Marroquín, F., Ramírez-Gómez, A., González-Montellano, C. et al. (2013). Experimental and numerical determination of mechanical properties of polygonal wood particles and their flow analysis in silos. *Granular Matter* 15: 811–826.

22 Lenaerts, B., Aertsen, T., Tijskens, E. et al. (2014). Simulation of grain–straw separation by discrete element modeling with bendable straw particles. *Computers and Electronics in Agriculture* 101: 24–33.

23 Thakur, S.C., Ooi, J.Y., and Ahmadian, H. (2016). Scaling of discrete element model parameters for cohesionless and cohesive solid. *Powder Technology* 293: 130–137.

24 Roessler, T. and Katterfeld, A. (2018). Scaling of the angle of repose test and its influence on the calibration of DEM parameters using upscaled particles. *Powder Technology* 330: 58–66.

25 Mohajeri, M.J., Helmons, R.L., van Rhee, C., and Schott, D.L. (2020a). A hybrid particle-geometric scaling approach for elasto-plastic adhesive DEM contact models. *Powder Technology* 369: 72–87.

26 Katterfeld, A., Donohue, T., and Ilic, D. (2012). Application of the discrete element method in mechanical conveying of bulk materials. In: *07th International Conference for Conveying and Handling of Particulate Solids*, 10–13 September 2012, Friedrichshafen, Germany.

27 Lommen, S., Schott, D.L., and Lodewijks, G. (2014). DEM speedup: stiffness effects on behaviour of bulk material. *Particuology* 12: 107–112.

28 Katterfeld, A., Coetzee, C., Donohue, T., et al. (2019). White Paper: Calibration of DEM parameters for cohesionless bulk materials under rapid flow conditions and low consolidation. https://www.researchgate.net/publication/334129169_Calibration_of_DEM_Parameters_for_Cohesionless_Bulk_Materials_under_Rapid_Flow_Conditions_and_Low_Consolidation.

29 Roessler, T. and Katterfeld, A. (2019a). DEM parameter calibration of cohesive bulk materials using a simple angle of repose test. *Particuology* 45: 105–115.

30 Tan, Y., Yu, Y., Fottner, J., and Kessler, S. (2021). Automated measurement of the numerical angle of repose (aMAoR) of biomass particles in EDEM with a novel algorithm. *Powder Technology* 388: 462–473.

31 Muller, D., Fimbinger, E., and Brand, C. (2021). Algorithm for the determination of the angle of repose in bulk material analysis. *Powder Technology* 373: 598–605.

32 Klanfar, M., Korman, T., Domitrovic, D., and Herceg, V. (2021). Testing the novel method for angle of repose measurement based on area-weighted average slope of a triangular mesh. *Powder Technology* 387: 396–405.

33 Qi, L., Chen, Y., and Sadek, M. (2019). Simulations of soil flow properties using the discrete element method (DEM). *Computers and Electronics in Agriculture* 157: 254–260.

34 Zhou, L., Yu, J., Liang, L. et al. (2021). DEM parameter calibration of maize seeds and the effect of rolling friction. *Processes* 9 (914): https://doi.org/10.3390/pr9060914.

35 Do, H.Q., Aragon, A.M., and Schott, D.L. (2018). A calibration framework for discrete element model parameters using genetic algorithms. *Advanced Powder Technology* 29: 1393–1403.

36 Derakhshani, S.M., Schott, D.L., and Lodewijks, G. (2015). Micro macro properties of quartz sand: experimental investigation and DEM simulation. *Powder Technology* 269: 127–138.

37 Elskamp, F., Kruggel-Emden, H., Henning, M., and Teipel, U. (2017). A strategy to determine DEM parameters for spherical and non-spherical particles. *Granular Matter* 19 (46): 1–13.

38 Horabik, J., Parafinuik, P., and Molenda, M. (2017). Discrete element modelling study of force distribution in a 3D pile of spherical particles. *Powder Technology* 312: 194–203.

39 Wang, L., Li, R., Wu, B. et al. (2018). Determination of the coefficient of rolling friction of an irregularly shaped maize particle group using physical experiment and simulations. *Particuology* 38: 185–195.

40 Fu, J.-J., Chen, C., Ferellec, J.-F., and Yang, J. (2020). Effect of particle shape on repose angle based on hopper flow test and discrete element method. *Advances in Civil Engineering* 2020: 8811063. https://doi.org/10.1155/2020/8811063.

41 Chen, Z., Wassgren, C., Veikle, E., and Ambrose, K. (2020). Determination of material and interaction properties of maize and wheat kernels for DEM simulation. *Biosystems Engineering* 195: 208–226.

42 Lommen, S., Mohajeri, M., Lodewijks, G., and Schott, D. (2019). DEM particle upscaling for large-scale bulk handling equipment and material interaction. *Powder Technology* 352: 273–282.

43 Pachon-Morales, J., Do, H., Colin, J. et al. (2019). DEM modelling for flow of cohesive lignocellulosic biomass powders: model calibration using bulk tests. *Advanced Powder Technology* 30: 732–450.

44 Coetzee, C.J. (2019). Particle upscaling: calibration and validation of the discrete element method. *Powder Technology* 344: 487–503.

45 Rong, W., Feng, Y., Schwartz, P. et al. (2020). Sensitivity analysis of particle contact parameters for DEM simulation in a rotating drum using response surface methodology. *Powder Technology* 362: 604–614.

46 Balevicius, R., Kacianauskas, R., Mroz, Z., and Sielamowicz, I. (2006). Discrete element method applied to multiobjective optimization of discharge flow parameters in hoppers. *Structural and Multidisciplinary Optimization* 31: 163–175.

47 Hlosta, J., Jezerská, L., Rozbroj, J. et al. (2020). DEM investigation of the influence of particulate properties and operating conditions on the mixing process in rotary drums: part 1 – determination of the DEM parameters and calibration process. *Processes* 8 (222): https://doi.org/10.3390/pr8020222.

48 Coetzee, C. and Nel, R. (2014). Calibration of discrete element properties and the modelling of packed rock beds. *Powder Technology* 264: 332–342.

49 Grima, A.P. and Wypych, P.W. (2011). Development and validation of calibration methods for discrete element modelling. *Granular Matter* 13: 127–132.

50 Zhou, Y.C., Xu, B.H., Yu, A.B., and Zulli, P. (2002). An experimental and numerical study of the angle of repose of coarse spheres. *Powder Technology* 125: 45–54.

51 Barrios, G.K.P., de Carvalho, R.M., Kwade, A., and Tavares, L.M. (2013). Contact parameter estimation for DEM simulation of iron ore pellet handling Gabriel. *Powder Technology* 248: 84–93.

52 Agarwal, A., Tripathi, A., Tripathi, A. et al. (2021). Rolling friction measurement of slightly non-spherical particles using direct experiments and image analysis. *Granular Matter* 23 (60): 1–14.

53 ASTM D3080/D3080M (2011). *Standard test method for direct shear test of soils under consolidated drained conditions*. West Conshohocken, PA: ASTM International.

54 ISO 17892-10:2018(2018). Geotechnical investigation and testing — Laboratory testing of soil — Part 10: Direct shear tests.

55 ASTM D6773-16 (2016). *Standard test method for bulk solids using schulze ring shear tester*.

56 Simons, T.A.H., Weiler, R., Strege, S. et al. (2015). A ring shear tester as calibration experiment for DEM simulations in agitated mixers – a sensitivity study. *Procedia Engineering* 102: 741–748.

57 Mohajeri, M.J., Do, H.Q., and Schott, D.L. (2020b). DEM calibration of cohesive material in the ring shear test by applying a genetic algorithm framework. *Advanced Powder Technology* 31 (5): 1838–1850.

58 Bian, X., Li, W., Qian, Y., and Tutumluer, E. (2019). Micromechanical particle interactions in railway ballast through DEM simulations of direct shear tests. *International Journal of Geomechanics* 19 (5): 1–19.

59 Falke, T., de Payrebrune, K.M., Kirchhof, S. et al. (2018). An alternative DEM parameter identification procedure based on experimental investigation: a case study of a ring shear cell. *Powder Technology* 328: 227–234.

60 Grima, A. and Wypych, P. (2013). Effect of particle properties on the discrete element simulation of wall friction. In: *ICBMH 2013 - 11th International Conference on Bulk Materials Storage, Handling and Transportation*.

61 Thakur, S.C., Ahmadian, H., Sun, J., and Ooi, J.Y. (2014). An experimental and numerical study of packing, compression, and caking behaviour of detergent powders. *Particuology* 12: 2–12.

62 Donohue, T.J., Wensrich, C.M., and Reid, S. (2016). On the use of the uniaxial shear test for DEM calibration. In: *The 7th International Conference on Discrete Element Methods*. China: Dalian (1–4 August 2016).

63 Yurata, T., Gidaspow, D., Piumsomboon, P., and Chalermsinsuwan, B. (2021). The importance of parameter-dependent coefficient of restitution in discrete element method simulations. *Advanced Powder Technology* 32: 1004–1012.

64 Hastie, D.B. (2013). Experimental measurement of the coefficient of restitution of irregular shaped particles impacting on horizontal surfaces. *Chemical Engineering Science* 101: 828–836.

65 Hlosta, J., Zurovec, D., Rozbroj, J. et al. (2018). Experimental determination of particle–particle restitution coefficient via double pendulum method. *Chemical Engineering Research and Design* 135: 222–233.

66 Mohajeri, M., van Rhee, C., and Schott, D.L. (2018). Penetration resistance of cohesive iron ore: a DEM study. In: *9th International Conference on Conveying and Handling of Particulate Solids, CHoPS 2018*.

67 Mohajeri, M.J., de Kluijver, W., Helmons, R.L.J. et al. (2021a). A validated co-simulation of grab and moist iron ore cargo: replicating the cohesive and stress-history dependent behaviour of bulk solids. *Advanced Powder Technology* 32 (4): 1157–1169.

68 Grima, A.P. (2011). Quantifying and modelling mechanisms of flow in cohesionless and cohesive granular materials. PhD thesis. University of Wollongong.

69 Katterfeld, A., Roessler, T., and Chen, W. (2018). Calibration of the DEM parameters of cohesive bulk materials for the optimisation of transfer chutes. In: *CHoPS 2018, 9th International Conference on Conveying and Handling of Particulate Solids*. (10th–14th September 2018).

70 Ajmal, M., Roessler, T., Richter, C., and Katterfeld, A. (2020). Calibration of cohesive DEM parameters under rapid flow conditions and low consolidation stresses. *Powder Technology* 374: 22–32.

71 Mohajeri, M.J., van Rhee, C., and Schott, D.L. (2021b). Replicating cohesive and stress-history-dependent behavior of bulk solids: feasibility and definiteness in DEM calibration procedure. *Advanced Powder Technology* 32: 1532–1548.

72 Carr, M.J., Chen, W., Williams, K., and Katterfeld, A. (2016). Comparative investigation on modelling wet and sticky material behaviours with a simplified JKR cohesion model and liquid bridging cohesion model in DEM. In: *ICBMH 2016 - 12th International Conference on Bulk Materials Storage, Handling and Transportation, Proceedings*.

73 Carr, M.J., Roessler, T., Otto, H. et al. (2019). Calibration procedure of discrete element method (DEM) parameters for cohesive bulk materials. In: *13th International Conference on Bulk Materials Storage, Handling & Transportation*.

74 Richter, C., Roessler, T., Kunze, G. et al. (2019). Development of a standard calibration procedure for the DEM parameters of cohesionless bulk materials – part II: efficient optimization-based calibration. *Powder Technology* 360: 967–976. https://doi.org/10.1016/j.powtec.2019.10.052.

75 Hess, G., Richter, C., and Katterfeld, A. (2016). Simulation of the dynamic interaction between bulk material and heavy equipment - calibration and validation. In: *ICBMH 2016: 12th International Conference on Bulk Materials Storage, Handling and Transportation; Proceedings, 11–14 July 2016* (ed. D. Hastie), 427–436. Darwin, Australia: The Institution of Engineers.

76 Rackl, M. and Hanley, K.J. (2016). A methodical calibration procedure for discrete element models. *Powder Technology* 307: 73–83. https://doi.org/10.1016/j.powtec.2016.11.048.

77 Benvenuti, L., Kloss, C., and Pirker, S. (2016). Identification of DEM simulation parameters by Artificial Neural Networks and bulk experiments. *Powder Technology* 291: 456–465. https://doi.org/10.1016/j.powtec.2016.01.003.

78 Hartmann, P., Cheng, H., and Thoeni, K. (2021). Performance study of iterative Bayesian filtering to develop an efficient calibration framework for DEM. *Computers and Geotechnics* 141: https://doi.org/10.1016/j.compgeo.2021.104491.

79 Richter, C. and Will, F. (2021). Introducing metamodel-based global calibration of material-specific simulation parameters for discrete element method. *Minerals* 11: 848. https://doi.org/10.3390/min11080848.